The atomic structure of the (111) surface of the antiferromagnetic 1/1 Au-Al-Tb approximant

Sam Coates
Department of Materials Science and Technology, Tokyo University of Science, 6 Chome–3–1 Niijuku, Katsushika City, Tokyo 125-8585

Kazuki Nozawa
Department of Physics and Astronomy, Kagoshima University 1-21-35, Korimoto, Kagoshima 890-0065, Japan

Masahiro Fukami and Kazuki Inagaki
Department of Materials Science and Technology, Tokyo University of Science, 6 Chome–3–1 Niijuku, Katsushika City, Tokyo 125–8585

Masahiko Shimoda
National Institute of Materials Science, Research Center for Advanced Measurement, 1-2-1 Sengen, Tsukuba, Ibaraki, 305–0047

Ronan McGrath and Hem Raj Sharma
Surface Science Research Centre and Department of Physics, University of Liverpool, Liverpool, L69 3BX, UK

Ryuji Tamura
Department of Materials Science and Technology, Tokyo University of Science, 6 Chome–3–1 Niijuku, Katsushika City, Tokyo 125-8585

The recently discovered antiferromagnetic 1/1 Au–Al–Tb approximant exhibits a whirling spin order oriented along the [111] direction. Here, we report an investigation of the atomic structure of the (111) surface by scanning tunnelling microscopy (STM) and density functional theory (DFT) calculations. STM reveals a Tb–terminated step–terrace morphology, with step heights appearing to minimize the number of 'broken' bulk icosahedra. The atomic structure of the terraces is bias dependent, with Tb atoms imaged under positive bias and Au/Al atoms under negative bias. The surface is found to reconstruct, with the Au/Al atoms producing a linear row structure, the first example of a surface reconstruction in a Tsai–type system. These observations are confirmed by DFT calculations.

I. INTRODUCTION

A potential route to discovering long–range magnetic order in quasicrystals lies in the stoichiometric manipulation of their periodic analogues, or, "approximants". Recent reports detail how composition can affect the type of magnetic order in Au–based approximants, with antiferromagnetic order evident in approximants of increasing complexity [1–3]. These approximants belong to a family of complex intermetallics known as Tsai–types, so called for their building block in the bulk, the Tsai–type cluster [4]. As Tsai–type approximants and quasicrystals share this same essential component, it is hoped that further manipulation may result in the synthesis of quasicrystal with long–range magnetic order.

The Tsai–type cluster is formed by a system of 5 hierarchical shells as shown in Figure 1(a), where a tetrahedron (grey) is enclosed by a dodecahedron (yellow), icosahedron (green), icosidodecahedron (blue), and finally a rhombic triacontahedron (red). In this scheme, rare–earth (RE) atoms solely occupy the vertices of the icosahedron shell (green in Figure 1(a)), whilst the other atoms occupy the vertices of the remaining shells (and the mid–edge points of the 5^{th} shell) [4, 5]. In quasicrystals, these clusters are distributed quasiperiodically, while in approximants, they decorate the lattice points of the crystal structure. The understanding of the structure of Tsai–type materials allows for in–depth interpretations of phase–specific and stoichiometric–specific properties, including magnetic transitions [2, 3, 6], novel electronic properties [7–9], and superconductivity [10–12].

For example, it has been reported recently that the spin structure of the antiferromagnetic 1/1 Au–Al–Tb

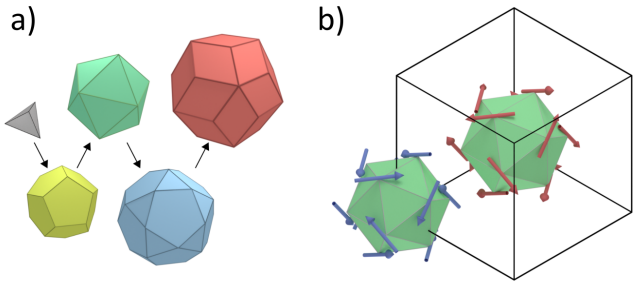

FIG. 1: **(a)** Tsai–cluster model of hierarchical shells. A tetrahedron (grey) is contained within a dodecahedron (yellow), icosahedron (green), icosidodecahedron (blue), and a rhombic triacontahedron (red). **(b)** Orthographic projection along the [111] direction of the 1/1 Au–Al–Tb unit cell, showing the spins of the origin and body–centre icosahedra.

approximant can be described by the spin vectors of Tb atoms of individual icosahedra. Each spin vector is rotated ∼86° with respect to the positional vector which describes the atomic position, relative to the centre of each icosahedra [13]. Icosahedra at the body–centre and origin exhibit opposite spins, hence producing long–range antiferromagnetic order. The resultant magnetic structure can be described as a 'whirling' spin order along the [111] direction. Figure 1(b) demonstrates an orthographic view of the [111] direction, showing origin and body–centre icosahedra, with spin vectors shown in blue and red respectively. Equivalent positions on the icosahedra exhibit opposite spin.

It is, therefore, of obvious interest to characterize the magnetic properties of the (111) surface. As a starting point, we investigate the atomic structure of the (111) surface. This will allow for an understanding of the magnetic surface structure, and also presents an opportunity to study a hitherto unreported surface of a Tsai–type approximant. In general, approximants have received comparatively less attention [14–16] than the high–symmetry surfaces of Tsai–type quasicrystals, which have been extensively studied, with considerable effort made to understand both surface structure and surface chemistry [17–29].

We find that the surface (111) surface of 1/1 Au–Al–Tb terminates at bulk planes containing Tb atoms. In addition, the step–terrace structure is determined by the minimization of the number of truncated Tsai–cluster icosahedra. Furthermore, we show that the Au/Al atoms of the surface form a row–like reconstruction, the first example of such a phenomenon at a Tsai–type material surface.

II. METHODS

High purity Au (4N), Al (4N) and Tb (3N) raw materials of the nominal composition $Au_{71}Al_{19}Tb_{10}$ were melted at 1273 K for 3 hours inside an alumina crucible under vacuum. Single grains were prepared using the self–flux method and the specimen was slowly cooled to 1003 K at a rate of 3 K/min. Single grains were separated from the molten flux using a centrifuge. The characterization of single grains was performed by X–ray diffraction on pulverized powder. The X–ray diffraction pattern shows that the obtained single grains are single 1/1 approximant phases with a=1.47581 nm. From the relationship between the lattice parameter and the composition, obtained for the polygrain 1/1 Au–Al–Tb approximants, the composition of the single grains is estimated to be $Au_{70}Al_{16}Tb_{14}$, which falls inside the antiferromagnetic region. The magnetic susceptibility χ of single grains was measured in the temperature range between 2 and 300 K using a magnetic property measurement system (MPMS; Quantum Design). A sharp cusp in χ–T due to an antiferromagnetic transition is observed at the Néel temperature $T_N = 11.9$ K. Thus, antiferromagnetic single grains with $T_N = 11.9$ K were successfully obtained in the present work.

The (111) surface of a single crystal of 1/1 Au–Al–Tb was polished with successively finer grades of diamond paste (6–0.25 μm) before washing in methanol. The surface was then further cleaned with sputter–anneal cycles (30 minute Ar^+ sputter, 2 hour anneal at 730 K) under ultra–high vacuum conditions. Substrate cleanliness was monitored with room temperature scanning tunnelling microscopy (STM). Using X-ray spectroscopy (XPS), it was found that after sputtering Al is preferentially removed from the surface, being the lightest element. However, a bulk –like starting composition is restored after the annealing process, indicating that no phase change has occurred. Similar phenomena was observed in Al–based quasicrystals [30]. As this is above T_N, the sample is in a paramagnetic phase. Bias conditions are referred to with respect to the STM tip, so that positive bias images unoccupied states and vice versa.

Calculations on the surface structure are based on density functional theory using the plane–wave basis set implemented in the Vienna Ab–initio Simulation Package [31]. The electron–ion interactions were described by the projector augmented–wave potentials [32] with the exchange–correlation functional in the generalized gradient approximation proposed by Perdew et al. [33]. The localized 4f–electrons of Tb were kept frozen in the core. The basis set contains plane-waves with a kinetic energy up to 240 eV. We performed non–spin–polarized calculations, since no significant difference in the surface atomic structure was observed in the spin-polarized cal-

culations carried out for comparison. The surface is approximated by a repeated slab model composed of an atomic layer of about 0.8nm and vacuum layer of over 1.2 nm. The Brillouin zone was sampled by a 1×5×5 Monkhorst–Pack grid yielding 13 irreducible k–points. The atomic positions were optimized using the calculated Hellman–Feynman forces and conjugate gradient method excepting the atoms located at the bottom of the atomic layer assumed as the bulk. The convergence criteria of 10^{-5} and 10^{-4} eV were applied for the electronic and ionic loops respectively. Simulated STM images were calculated within the Tersoff–Hamann approximation [34].

III. RESULTS AND DISCUSSION

A. Step Morphology

Figure 2(a) shows a large scale STM image of the surface, where a step–terrace morphology is observed. A terrace kink angle α is marked, with a value of $119 \pm 2°$, consistent with 3–fold symmetry expected from the bulk model structure. Figure 2(b) shows a histogram taken from Figure 2(a), illustrating the distribution of step heights, with the most common step height measured as 1.22 ± 0.04 nm. Island–like protrusions are regularly observed on top of the terraces, with examples circled in white. The heights of these islands are between 0.3–0.4 nm, with no defined morphology evident. The width of individual terraces rarely exceeds 100 nm, independent of annealing conditions. The islands and small terrace size therefore suggests a low stability in comparison to, for example, the 3–fold surface of *i*–Ag–In–Yb (the quasicrystalline analogue), which produces flat terraces with widths upwards of 300 nm.

We consider the step–heights in terms of planes of atoms in the bulk model. Figure 2(c) shows a side–view of the Tb planes in the bulk, arranged perpendicular to the [111] direction. Three Tb planes form what we will refer to as Tb surface slabs, examples of which are bounded by black boxes. The separation of these slabs (i.e. centre to centre) is 0.43 nm. Therefore, the measured step height can be considered as the separation between four slabs, 1.28 nm, as indicated at the bottom of Figure 2(c). It should be noted that this value and the measured step height (1.22 nm) are 1.5 times larger than the separation of adjacent lattice planes in the bulk $d = \frac{a}{\sqrt{h^2+k^2+l^2}} = 0.8521$ nm (where $a = 1.4758$ nm [2]). A possible explanation for the large step height will be discussed later.

Every Tsai–type quasicrystal surface studied by STM has found to be rare–earth (RE) atom terminated, that is, the surface planes are densely populated by rare earth atoms [18, 19, 23]. This has been linked to both the low surface free energy and low–lying unoccupied 3d states of the RE atoms which act to stabilize the surface [23, 35, 36]. Despite lack of atomic resolution on the Ag–In–RE(100) approximant surfaces (RE = Yb, Tb, Gd), it was regarded as likely that it is also true for these cases [16]. Therefore, the step heights for the (111)Au–Al–Tb surface are considered in terms of Tb dense planes.

B. Atomic Structure

1. *Positive bias and spin structure*

The structure of the surface can be resolved with sub–cluster (but not atomic) resolution. First, we consider positive bias images, Figures 3(a, b). Figure 3(a) shows a set of dimer–like bright protrusions which are arranged in a rhombohedral surface unit cell with lattice parameters $a = 2.12 \pm 0.07$ nm, $b = 2.10 \pm 0.04$ nm, and $\alpha = 58 \pm 2°$ where the marked vectors intersect the centre–point of the dimers. An example of adjacent protrusions in the dimers are highlighted by an oval, which are separated by 1.23 ± 0.03 nm. The dimers can also be considered as forming hexagons enclosing an area of dark contrast, highlighted by the black hexagon.

Figure 3(b) shows a different area of the surface observed at the same bias value as Figure 3(a). The apparent change in morphology, where the dark centres of the hexagons in Figure 3(a) are resolved as low intensity protrusions, may arise from a change in tip/tunnelling conditions. A rhombohedral cell which includes the below–plane protrusion in the hexagon has parameters of $c = 1.23 \pm 0.07$ nm, $d = 1.24 \pm 0.08$ nm, and $\beta = 61 \pm 2°$.

In previous work on Tsai–type quasicrystal and approximant surfaces, rare–earth atoms are detected under positive bias conditions [18, 19, 23, 29]. Therefore, we consider similar behaviour in our analysis. As previously discussed, the Tb slabs used to explain the step heights consist of three closely separated Tb planes, Figure 2(c). The structure observed in Figure 3(a) can be understood using the centre of these three planes. Figure 3(c) shows a model of this plane, which consists of sets of Tb atoms arranged in triangles with edge lengths 0.55 nm, rotated 60° with respect to each other. These triangles are canted with respect to the surface vectors by $\sim 7°$. The rhombohedral and hexagonal cells highlighted in Figure 3(a) are also marked in Figure 3(c), where each bright protrusion observed corresponds to an individual triangle. The model rhombohedral unit cell gives values of $a = b = 2.09$ nm, a good fit with the experimental value.

The alternative positive–bias structure observed in Figure 3(b) can be explained by the tip tunnelling to the lowest Tb plane in the slab. This plane consists of larger edge length Tb triangles (0.9 nm) with only one orientation, and is shown in addition to the middle Tb

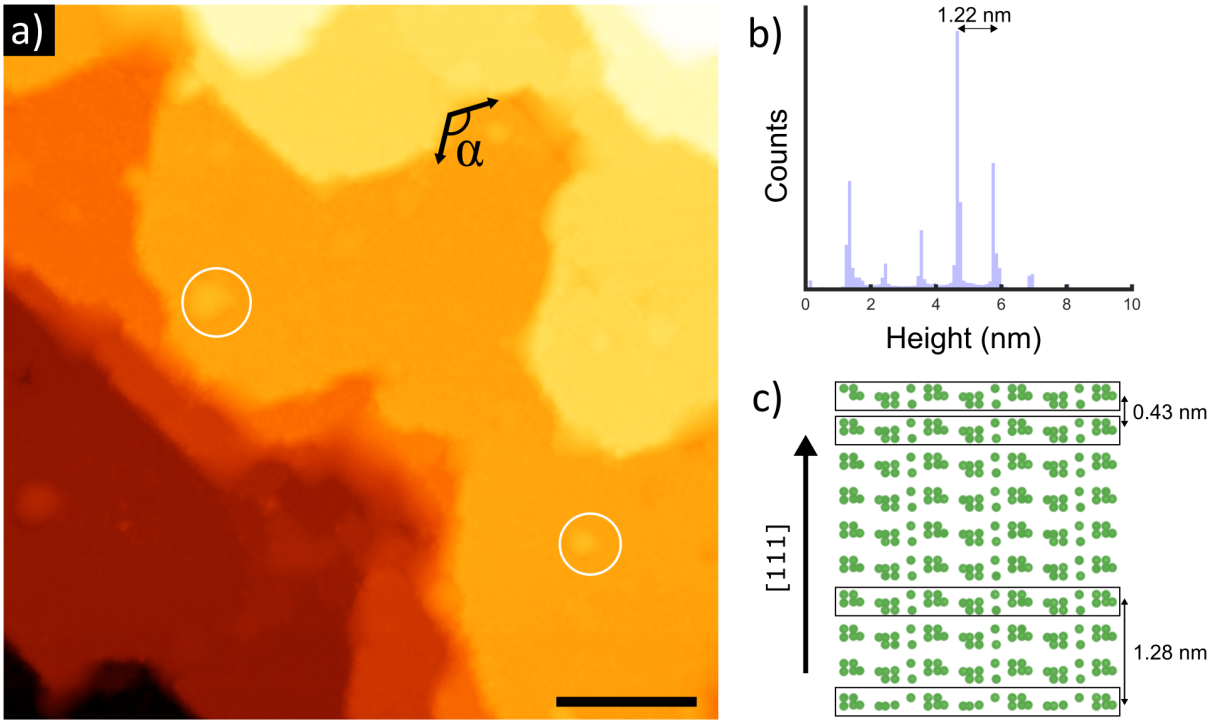

FIG. 2: **(a)** STM image (V_b = 2 V, I_t = 172 pA) of the step terrace structure of the (111) surface. α indicates the terrace kink angle. White circles mark islands. Scale bar is 30 nm. **(b)** A histogram taken from (a), showing the step height distribution. The average step height is labelled. **(c)** Bulk model of Tb planes arranged along the [111] direction. Groups of three planes are separated by 0.43 nm, as labelled. Groups of planes which correspond to the measured step height are also indicated.

plane in Figure 3(d) where examples of the larger triangles are highlighted. A dashed rhombohedron indicates the projected bulk unit cell. Dashed circles indicate the protrusions measured by STM. The addition of these triangles forms a small rhombohedral cell as highlighted, with dimensions commensurate with the experimental values $c = d = 1.21$ nm. As the structures observed in Figure 3(a, b) can be explained using only the bottom two planes of a Tb slab, we infer that the surface terminates at the middle Tb plane. A possible explanation for this plane 'selection' will be discussed later.

As the Tb atoms carry the magnetic order of the sample, we can visualize the resultant spin structure of the two surface Tb planes below T_N using the previously described structure taken from [13]. We can also consider the magnetic structure as two inter–penetrating simple cubic lattices, each of which are decorated by one 'type' of spin icosahedron (i.e. one of the two icosahedra in Figure 1(b)). We will broadly describe these as either 'up' or 'down' icosahedra to simply differentiate their spin structure.

Using the observed step height as a guide, we can truncate the bulk spin model at one of two terraces. These terraces exhibit opposing spins. Figure 3(e, f) shows the spin structure of the hexagons highlighted in Figures 3(b, d). Coloured arrows denote spins from either an up icosahedra (blue), or a down icosahedra (red). The small triangles of the top Tb plane are formed by up (down) icosahedra, whilst the larger triangles of the Tb plane below are formed by down (up) icosahedra. Adjacent small triangles show sets of spins rotated by 60°. As the spin vectors are canted with respect to their position vectors, the spins are not exactly parallel/perpendicular with the surface direction, as indicated by the planar views at the bottom of Figures 3(e, f).

2. *Negative bias and reconstruction*

Figures 4(a) shows the surface as imaged with negative bias, where a bright row structure with overall 2–fold symmetry is observed. We note that this surface morphology is observed for a range of bias conditions (i.e. -2000 to ∼1000 mV). Swapping between large bias polarities in the same area of the sample (i.e. -1900 to 1900 mV) confirms that this row morphology is not an impurity phase i.e. it is possible to reproduce the structure in Figures 3(a, b) simply by switching to a high

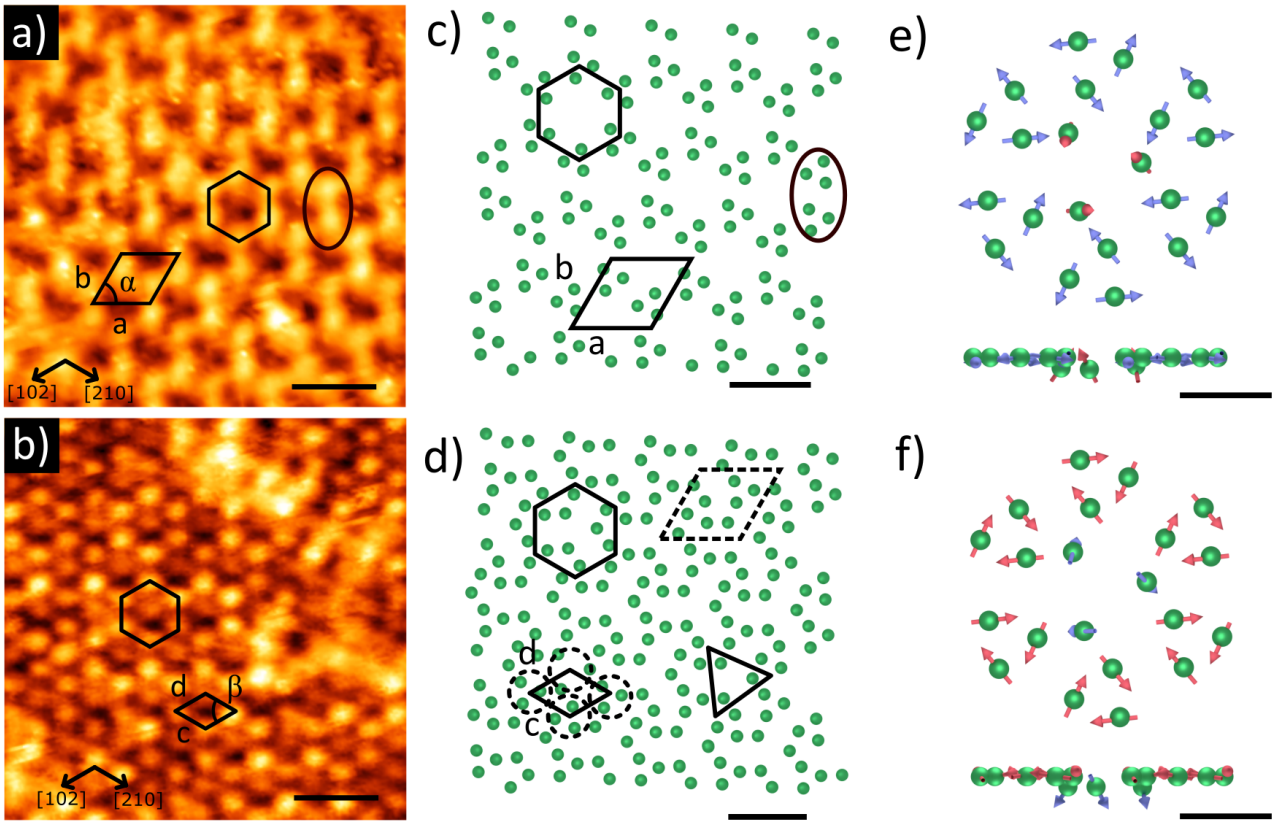

FIG. 3: **(a)** STM image ($V_b = 1900$ mV, $I_t = 175$ pA) showing the atomic structure of a terrace. Bright dimer–like protrusions (highlighted by an oval) form a rhombohedral unit cell or hexagonal structure, both marked. Crystallographic direction is marked. Scale bar is 3 nm. **(b)** STM image ($V_b = 1900$ mV, $I_t = 172$ pA) showing additional features which appear dependent on tip condition. Again a rhombohedral and hexagonal cell are marked. Crystallographic direction is marked. Scale bar is 3 nm. **(c)** A model schematic of Tb atoms (green) forming the structure in **(a)**. The corresponding features (oval, rhombohedron, hexagon) are marked. Scale bar is 3 nm. **(d)** The model structure used to explain the additional feature in **(b)**. Scale bar is 3 nm. **(e, f)** The resultant spin structures of the hexagon highlighted in **b, d** at two different terraces. Arrows denote the spin direction, whilst the colour indicates the type of icosahedron responsible for the spin. Planar views are shown below. Scale bars are 1 nm.

positive bias. Likewise, the row directions are independent of scanning direction or tip condition, as confirmed by rotating the scan orientation and undertaking multiple tip–cleaning procedures. Therefore, we consider this morphology as a result of a surface reconstruction.

The distance between adjacent rows is 1.06 ± 0.09 nm. A 'V'–shaped protrusion is highlighted by a black circle, which forms a marked rhombohedral unit cell between the bright rows, with parameters $a = 2.09 \pm 0.06$ nm, $b = 2.15 \pm 0.04$ nm, i.e. the same unit cell dimensions as in Figure 4(c). Inside the marked unit cell is a section of a bright row. Occasionally a feature will 'bridge' between two rows: an example is circled in white which will be discussed later. A fast Fourier transform (FFT) of Figure 4(a) is shown in Figure 4(b) to demonstrate the symmetry of the morphology observed. Here, the expected 6–fold symmetry from a (111) surface termination is shown by the set of spots highlighted by the coloured circles, which are arranged in a hexagon. However, the intensity of the spots varies, as made evident by comparing those circled in blue to those circled in green. The brighter spots reflect the 2–fold nature of the rows, while the entire set of spots indicate that there is a 3–fold symmetric network embedded within the row structure, i.e. the 'V'–shaped protrusions.

We analyse the observed structure using Au/Al atoms contained within the surface slab used to explain Figures 3(a,b). As a 2–fold row structure cannot be obtained by a simple bulk truncation, we instead consider a missing–row structure in which several atoms of the unit cell in the topmost plane are removed. It is presumed that these atoms desorb, are incorporated at step edges via diffusion during the cleaning process, or are perhaps visible as the bright island–type defects highlighted in

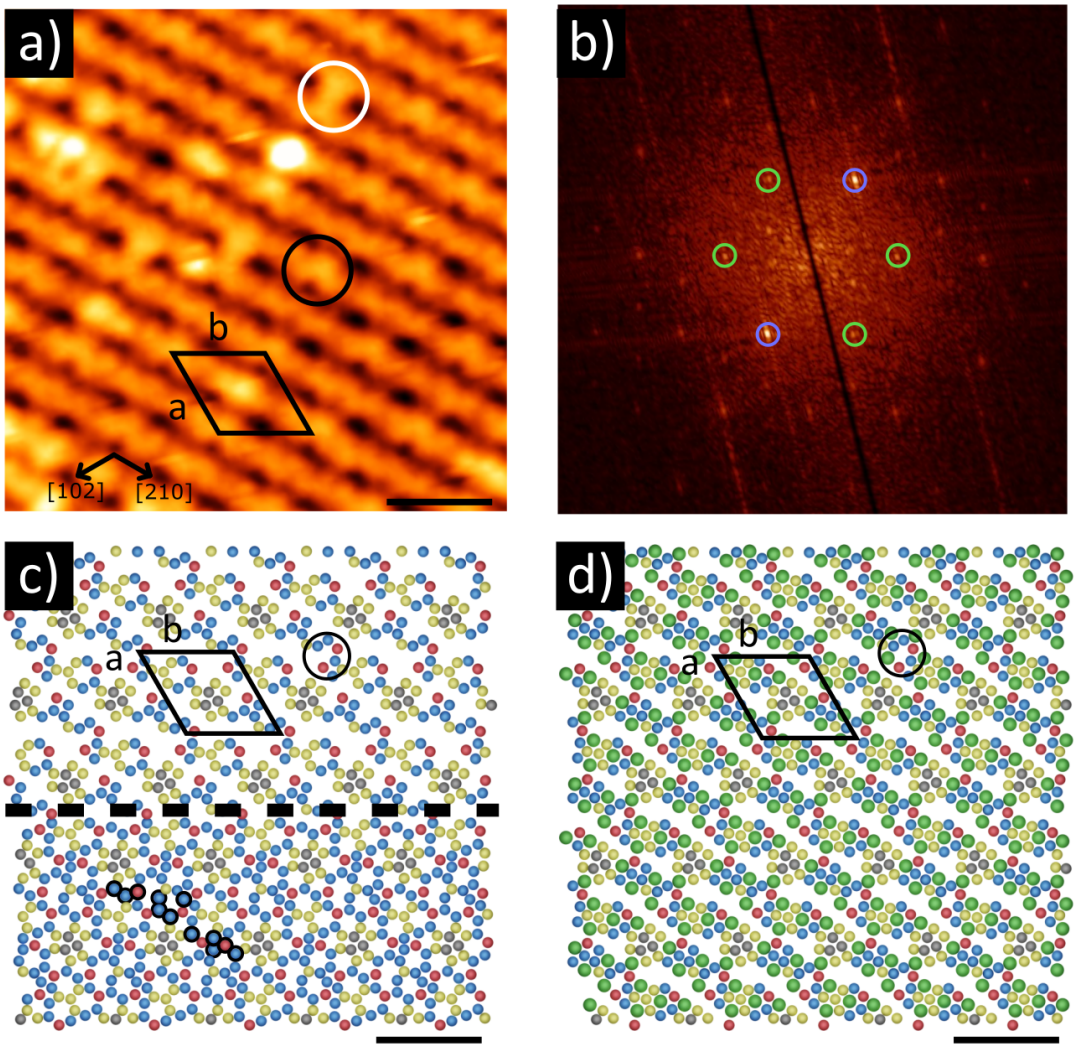

FIG. 4: **(a)** STM image (V_b = -1000 mV, I_t = 140 pA) of the terrace morphology under negative bias. A rhombohedral unit cell is marked, linking V–shaped protrusions, one of which is circled in black. Crystallographic direction is marked. Scale bar is 3 nm. **(b)** An FFT of (a), where spots are highlighted by circles, showing the 6–fold symmetry of the distribution of the V protrusions. The blue circles mark spots of increased intensity, indicating the 2–fold symmetry of the rows. **(c)** Model schematic of **(a)**. Red, blue, yellow, and grey circles indicate 5^{th}, 4^{th}, 2^{nd}, and 1^{st} shell positions of Au/Al atoms. The bulk truncated model is shown below the dashed line. A set of individual atoms are circled, indicating which atoms are removed under the reconstruction. Above the dashed line, the rhombohedral unit cell and V–shaped protrusions of (**a**) are marked. Scale bar is 3 nm. **(d)** Model slab of the surface including Tb atoms. The rhombohedral unit cell and V–shaped protrusions of (**a**) are again marked. Scale bar is 3 nm.

Figure 2(a).

Figure 4(c) shows the surface model considering all non–Tb positions. Here, the atoms of each shell are represented as spheres and are coloured as in Figure 1(a). The bulk–truncated model is shown below the dashed line. A set of 12 atoms are highlighted by black circles, representing the atoms which are removed from the surface unit cell to obtain the surface reconstruction. The choice of these atoms was determined by a trial–and–error comparison between experimental and simulated STM images, which are discussed later. Above the dashed unit cell is the proposed reconstruction. The separation between adjacent rows is ∼1.05 nm, matching the experimentally observed value. A group of atoms is highlighted by a black circle, indicating the proposed origin of the 'V'–shaped protrusion. The marked unit cell joins 4 of these groups together, with $a = b = 2.09$ nm, again fitting with the experimental values. Likewise, in-

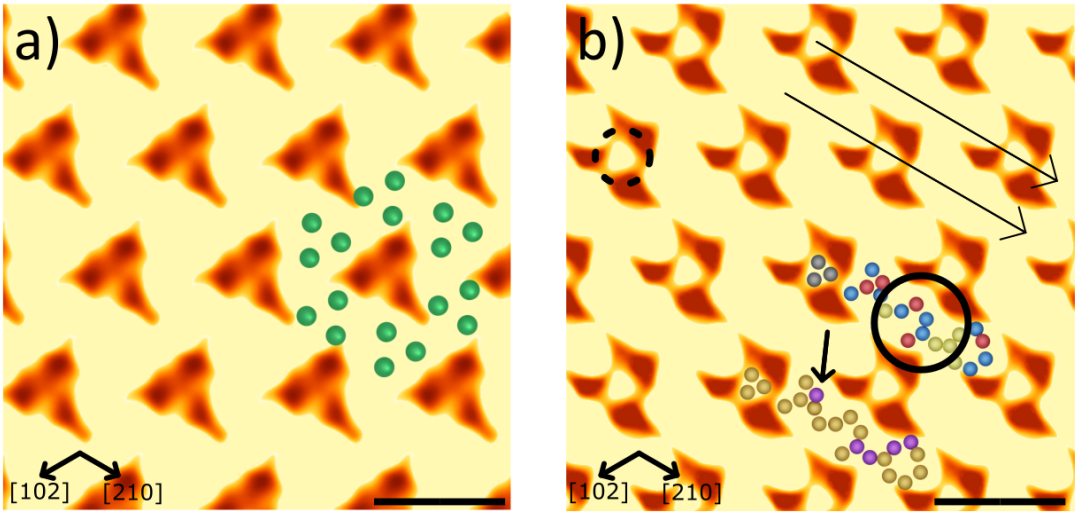

FIG. 5: **(a)** Simulated STM image V_b = +1900 mV. Bright circles form a hexagonal network matching the STM image of Figure 3(a). Overlaid are some of the Tb atoms which form the hexagonal structure. A dim triangle can be seen at the centre of the hexagon, i.e. from the lower Tb plane in Figure 3(d). Scale bar is 2 nm. **(b)** Simulated STM image at V_b = -1900 mV. The row structure as observed in Figure 4(a) is clearly seen, and indicated by two parallel arrows. Overlaid are sections of the reconstructed model; one section is coloured as with the Tsai type shells, the other is coloured to represent its chemistry i.e. Au is gold, and Al is purple. The V–shaped protrusion and 'bridging' feature in Figure 4(a) are indicated with a black circle and an arrow, respectively. A dashed circle indicates a protrusion from 1st shell atoms. Scale bar is 2 nm.

side the unit cell are a row of atoms which corresponds to the row inside the cell of Figure 4(a). The overall surface structure is therefore presented in Figure 4(d), comprised of a 3–fold network of Tb triangles within a 2–fold row structure of Au/Al atoms. The unit cell and V protrusion from Figure 4(c) are overlaid for comparison.

3. Simulated STM

To confirm the comparison between the model and the experimentally observed structure, STM images were simulated using a range of different surface models. Models were changed by removing different sets of Au/Al atoms from the unit cell, in addition to changing the chemistry of the atoms of the surface (i.e. switching between Au and Al at sites with nearly equivalent partial occupancy [2]). Before calculating the STM isosurface, each model was structurally relaxed and subsequent desorption energies were calculated. Often, the relaxations would lead to unstable Au/Al atoms and qualitatively ill–fitting models. Occasionally, Tb atoms were also shifted, leading to poor fits across all bias conditions. Calculations were performed with different Tb terminations i.e. either with all three Tb planes from the surface slab of Figure 2(c), or with the bottom two as shown in Figures 3(d), 4(d).

The model which produced the best fit, with no unstable surface atoms, is that shown in Figure 4(d). After a structural relaxation of this model, the isosurfaces for positive and negative bias were calculated. Figure 5(a) shows the result of the simulation for positive bias (+1900 mV). Bright protrusions match the dimer–like network observed in Figure 3(a). Overlaid are a series of Tb atoms, so that each protrusion of a hexagon is formed by a Tb triangle. The centre of the hexagon is dark, although a dim triangle can be seen. This corresponds to the larger Tb triangle of the lower Tb plane, as previously mentioned when discussing Figure 3(b).

Figure 5(b) shows the surface model as simulated under negative bias (-1900 mV). The structure observed matches that seen in Figure 4(a) i.e. rhombohedral overall, yet with a row structure. The rows are indicated by two long arrows. Overlaid on top of a section of a row, coloured as the Tsai cluster shells in Figure 1(a), are the Au/Al atoms which contribute to the observed local density of states (LDOS). A black circle indicates the group of atoms which forms the V–shaped protrusion in Figure 4(a). A dashed circle indicates a bright protrusion which appears separated from other LDOS contributions. According to the surface model, it is produced by atoms belonging to the 1st shell (i.e. the tetrahedron in Figure 1(a)) of the Tsai cluster. Typically, this shell is not considered in surface studies of Tsai–type materials, as

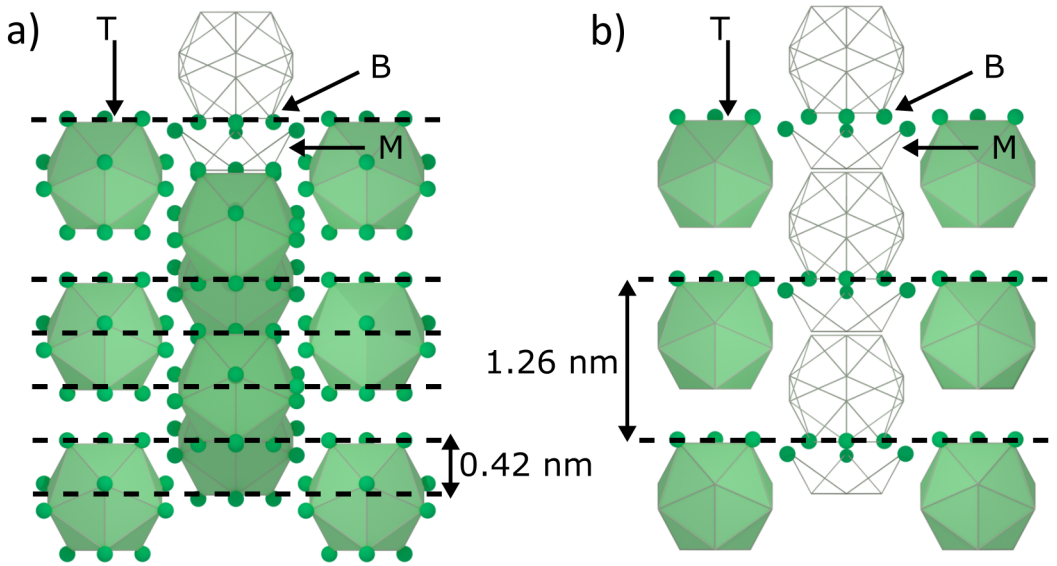

FIG. 6: **(a)** Bulk model of Tb atoms illustrating where surface terminations would truncate the Tb icosahedra, either top (T), bottom (B), or middle (M). Skeletal structures highlight the nature of the truncation. Dashed lines separated by 0.43 nm illustrate the minimum step height for Tb atoms. **(b)** The same schematic as **(a)**, altered to reflect the measured step height. The visible planes of Tb atoms are those in Figure 3(d).

its dynamism leads to an ill–defined surface contribution [37–39]. To represent the tetrahedron, we have assumed four Au atoms occupy non–adjacent vertices of a small cube, similar to the cubic unit cell of the bulk. There are two possible orientations of the tetrahedron: up and down, where one of the Au atoms occupy the (111) and (-1,-1,-1) vertices of the cube respectively. Changing the relative orientations of the tetrahedra has little to no effect on the calculated STM image, so we arbitrarily assign them as up–tetrahedra.

A second set of atoms is overlaid in Figure 5(b) which are coloured to represent their chemistry, so that Au atoms are gold and Al atoms are purple. The 'bridging' protrusion highlighted in white in Figure 4(a) is indicated by an arrow. As this feature is only occasionally seen by STM, it is presumed that atoms at or near this position are either partially removed during cleaning, or that the chemistry of the site changes (due to partial occupancy [2]) so that the LDOS contribution also changes.

4. Surface stability

Here we discuss the surface truncation and stability in comparison to quasicrystalline surfaces. The (111) surface of Au–Al–Tb is a periodic analogue to the 3–fold surface of a Tsai–type quasicrystal. On the 3–fold surface of *i*–Ag–In–Yb, terraces are formed at every so–called cluster–centre plane [19]. These are dense planes which contain the geometric centres of the Tsai clusters which form the bulk structure of the quasicrystal. These planes invariably produce a high density of RE atoms. As previously discussed, the stability of the surface termination has been linked to the RE atoms [19, 23, 35, 36].

The periodic interpretation of cluster–centre planes for the Au–Al–Tb(111) system would simply be the lattice points of the body–centred cubic structure. If Au–Al–Tb(111) were to be terminated at every cluster–centre plane, as with the quasicrystal, we would see step heights at every 0.43 nm ($0.5 \times d$), as demonstrated by the Tb slabs in Figure 2(c). If this were the case, adjacent terraces would display the same structure with a relative shift of $\sqrt{2}a$. Instead, we see separations of $1.5 \times d$. Again, the structure of adjacent terraces are identical except for the $\sqrt{2}a$ shift. Both geometrically and chemically, therefore, there is no difference between step heights of 0.5 and $1.5{\times}d$. The 'selection' of larger step heights suggests that there is another driving force for these step heights beyond the terrace constituents and their arrangement.

Figure 6(a) shows a section of the Tb atoms of the bulk structure along the [111] direction, i.e. an enlarged version of Figure 2(c). Here, the icosahedral shells which are used to model the atoms are included. Dashed black lines show prospective truncations at every cluster centre plane i.e. step heights of 0.43 nm. At the top of Figure 6(a) three icosahedra are marked by letters, indicating the positions on the icosahedra through which the plane

of truncation intersects. For instance, the icosahedron labelled as top (T) will donate its top atoms to the surface plane. The middle icosahedron (M), is broken just below its midpoint, whilst bottom (B) donates its bottom atoms. The top and bottom truncations each provide triangles of edge length 0.55 nm, i.e. the bright protrusions in Figures 3(a), 5(a). The middle icosahedra gives the larger Tb triangles in the lower plane, as described in Figure 3(d).

The icosahedra can also be considered in terms of how broken they are i.e. full (top), half–full (middle), or empty (bottom), as indicated by the skeletal structures in Figure 6(a). It follows that truncations at every 0.43 nm would produce the maximum number of broken icosahedra: if we study one icosahedron in Figure 6(a), we see that it could be 'truncated' three times. Figure 6(b) is an alternate version of Figure 6(a), which shows only the icosahedra involved in bulk truncations at every 1.28 nm, the experimentally observed step height. Some atoms have also been removed for clarity – the remaining atoms are those detected by STM in Figure 3. We suggest that this model shows a possible explanation for the enlarged step height, through the preservation of as many unbroken icosahedra as possible. To demonstrate, we calculate the number of whole icosahedra in a section of the bulk for each step height (i.e. 0.43 nm and 1.28 nm), for 5 step heights. To do so, we build a quasi–2–dimensional slice with one unit cell thickness, and 5 unit cells in width; the height of the slab is then determined by the step height value. Atoms are removed to simulate a step–terrace structure with 5 steps, and the number of whole icosahedra is counted. The larger step height value gives 2.5 times as many unbroken icosahedra in the bulk. This behaviour is contrary to the Tsai–type quasicrystalline system, and may indicate that in this system, or along this crystallographic direction, the role of a 'full' icosahedra has energetic implications as opposed to simply geometric. Such behaviour has been previously observed on, for example, *i*–Al–Pd–Mn [40].

IV. CONCLUSIONS

We have investigated the (111) surface of the antiferromagnetic 1/1 Au–Al–Tb approximant, finding that the surface is terminated at Tb–containing planes, with a step height that appears to promote the minimization of broken icosahedra in the bulk. As Tsai–type quasicrystals do not appear to follow this scheme, this behaviour could be investigated in the future on more complex Tsai–type approximants (i.e. 2/1), which contain all of the building blocks used to describe Tsai–type quasicrystals.

We have shown that there is a bias–dependency in the terrace structure of the surface, where at positive bias we resolve Tb atoms arranged in a rhombohedral or hexagonal fashion. At negative bias we resolve Au/Al atoms, which are found to form the first reconstruction observed on a Tsai–type material surface. These observations are confirmed using DFT calculations. The unique mixture of 2– and 3–fold symmetric surface constituents will be an intriguing playground for studying epitaxy and molecular adsorption.

ACKNOWLEDGEMENTS

This work was supported by a Kakenhi Grant-in-Aid (No. 19H05817, 19H05818) from the Japan Society for the Promotion of Science (JSPS). The DFT calculations have been done using the facilities of National Institute for Materials Science, Japan and the Institute for Solid State Physics, the University of Tokyo.

[1] A. Ishikawa, T. Hiroto, K. Tokiwa, T. Fujii, and R. Tamura, Composition-driven spin glass to ferromagnetic transition in the quasicrystal approximant Au-Al-Gd. Phys. Rev. B, 93, 024416 (2016).

[2] A. Ishikawa, T. Fujii, T. Takeuchi, T. Yamada, Y. Matsushita, and R. Tamura, Antiferromagnetic order is possible in ternary quasicrystal approximants. Phys. Rev. B, 98, 220403 (2018).

[3] S Yoshida, S Suzuki, T Yamada, T Fujii, A Ishikawa, and R Tamura. Antiferromagnetic order survives in the higher-order quasicrystal approximant, Phys. Rev. B, 100, 180409 (2019).

[4] H. Takakura, C. P. Gómez, A. Yamamoto, M. de Boissieu, and A. P. Tsai, Atomic structure of the binary icosahedral Yb–Cd quasicrystal. Nat. Mater., 6, 58 (2007).

[5] A. P. Tsai, J. Q. Guo, E. Abe, H. Takakura, and T. J. Sato, Alloys: A stable binary quasicrystal. Nature, 408, 537 (2000).

[6] R. Tamura, Y. Muro, T. Hiroto, K. Nishimoto, and T. Takabatake, Long-range magnetic order in the quasicrystalline approximant Cd_6Tb. Phys. Rev. B, 82, 220201 (2010).

[7] K. Deguchi, S. Matsukawa, N. K. Sato, T. Hattori, K. Ishida, H. Takakura, and T. Ishimasa, Quantum critical state in a magnetic quasicrystal. Nat. Mat., 11, 1013–1016 (2012).

[8] T. Watanuki, S. Kashimoto, D. Kawana, T. Yamazaki, A. Machida, Yukinori Tanaka, and Taku J. S, Intermediate-valence icosahedral Au-Al-Yb quasicrystal. Phys. Rev. B, 86, 094201 (2012).

[9] S. Jazbec, S. Vrtnik, Z. Jagličić, S. Kashimoto, J. Ivkov, P. Popčević, A. Smontara, H. J. Kim, J. G. Kim, and J. Dolinšek, Electronic density of states and metastability of icosahedral Au–Al–Yb quasicrystal. Journal of Alloys and Compounds, 586, 343–348 (2014).

[10] K. Kamiya, T. Takeuchi, N. Kabeya, N. Wada, T. Ishimasa, A. Ochiai, K. Deguchi, K. Imura, and N. K. Sato, Discovery of superconductivity in quasicrystal. Nat. Commun., 9, 1–8 (2018).

[11] K. Deguchi, M. Nakayama, S. Matsukawa, K. Imura, K. Tanaka, T. Ishimasa, and N. K. Sato, Crystal structure of superconducting 1/1 cubic Au–Ge–Yb approximant with Tsai-type cluster. Journal of the Physical Society of Japan, 84, 015002 (2015).

[12] K. Deguchi, M. Nakayama, S. Matsukawa, K. Imura, K. Tanaka, T. Ishimasa, and N. K. Sato, Superconductivity of Au–Ge–Yb approximants with Tsai-type clusters. Journal of the Physical Society of Japan, 84, 023705 (2015).

[13] T. J. Sato, A. Ishikawa, A. Sakurai, M. Hattori, M. Avdeev, and R. Tamura, Whirling spin order in the quasicrystal approximant $Au_72Al_14Tb_14$. Phys. Rev. B, 100, 054417 (2019).

[14] S. Hars, H. Sharma, J. Smerdon, T. Yadav, R. Tamura, M. Shimoda, and R. McGrath, The structure of the (100) surface of Ag-In-Gd 1/1 approximant. Acta Physica Polonica A, 126, 479–481 (2014).

[15] C. Cui, H. Sharma, P. Nugent, M. Shimoda, and A. P. Tsai, STM study on the (100) surface of the Ag-In-Yb 1/1 cubic approximant. Acta Physica Polonica A, 126, 577–580 (2014).

[16] S. S. Hars, H. R. Sharma, J. A. Smerdon, T. P. Yadav, A. Al-Mahboob, J. Ledieu, V. Fournée, R. Tamura, and R. McGrath, Surface structure of the Ag-In-(rare earth) complex intermetallics. Phys. Rev. B, 93, 205428 (2016).

[17] H. R. Sharma, M. Shimoda, S. Ohhashi, and A. P. Tsai, First UHV surface studies of single-grain icosahedral Ag–In–Yb quasicrystal. Philos. Mag., 87, 2989–2994 (2007).

[18] H. R. Sharma, M. Shimoda, K. Sagisaka, H. Takakura, J. A. Smerdon, P. J. Nugent, R. McGrath, D. Fujita, S. Ohhashi, and A. P. Tsai, Structure of the fivefold surface of the Ag-In-Yb icosahedral quasicrystal. Phys. Rev. B, 80, 121401 (2009).

[19] C. Cui, P. J. Nugent, M. Shimoda, J. Ledieu, V. Fournée, A. P. Tsai, R. McGrath, and H. R. Sharma, The atomic structure of the threefold surface of the icosahedral Ag–In–Yb quasicrystal. Journal of Physics: Condensed Matter, 24, 445011 (2012).

[20] P. J. Nugent, G. Simutis, V. R. Dhanak, R. McGrath, M. Shimoda, C. Cui, A. P. Tsai, and H. R. Sharma, Surface oxidation of the icosahedral Ag-In-Yb quasicrystal. Phys. Rev. B, 82, 014201 (2010).

[21] P. J. Nugent, J. A. Smerdon, R. McGrath, M. Shimoda, C. Cui, A. P. Tsai, and H. R. Sharma, Step-terrace morphology and reactivity to C_{60} of the five-fold icosahedral Ag–In–Yb quasicrystal. Philos. Mag., 91, 2862–2869 (2011).

[22] H. R. Sharma, K. Nozawa, J. A. Smerdon, P. J. Nugent, I. McLeod, V. R. Dhanak, M. Shimoda, Y. Ishii, A. P. Tsai, and R. McGrath, Templated three-dimensional growth of quasicrystalline lead. Nat. Commun., 4, 2715 (2013).

[23] C. Cui, P. J. Nugent, M. Shimoda, J. Ledieu, V. Fournée, A. P. Tsai, R. McGrath, and H. R. Sharma. Structure of the twofold surface of the icosahedral Ag–In–Yb quasicrystal. Journal of Physics: Condensed Matter, 26, 015001 (2013).

[24] J. A. Smerdon, K. M. Young, M. Lowe, S. S. Hars, T. P. Yadav, D. Hesp, V. R. Dhanak, A. P. Tsai, H. R. Sharma, and R. McGrath, Templated quasicrystalline molecular ordering. Nano Lett., 14, 1184–1189 (2014).

[25] C. Cui, M. Shimoda, and A. P. Tsai, Studies on icosahedral Ag–In–Yb: a prototype for Tsai-type quasicrystals. RSC Advances, 4, 46907–46921 (2014).

[26] H. R. Sharma, P. J. Nugent, T. C. Q. Noakes, J. Smerdon, J. Parle, A. P. Tsai, and R. McGrath, Medium energy ion scattering (MEIS) study from the five-fold surface of icosahedral Ag-In-Yb quasicrystal. Journal of Physics: Conference Series, 809, 012017 (2017).

[27] S. S. Hars, H. R. Sharma, J. A. Smerdon, S. Coates, K. Nozawa, A. P. Tsai, and R. McGrath, Growth of a bismuth thin film on the five-fold surface of the icosahedral Ag–In–Yb quasicrystal. Surf. Sci., 678, 222–227 (2018).

[28] S. Coates, S. Thorn, R. McGrath, H. R. Sharma, and A. P. Tsai, Unique growth mode observed in a pb thin film on the threefold surface of an i-Ag-In-Yb quasicrystal. Phys. Rev. Mater., 4, 026003 (2020).

[29] D. Burnie, S. Coates, R. McGrath, and Sharma H. R, Bias-voltage dependent STM images from the 2–fold surface of the icosahedral Ag-In-Yb quasicrystal. Journal of Physics: Conference Series, 1458, 012017 (2020).

[30] F. Samavat, M. J. Gladys, C. J. Jenks, T. A. Lograsso, B. V. King, and D. J. O'Connor, Study of preferential sputtering and segregation effects on the surface composition of Al– Pd–Mn quasi-crystals. Surface and Interface Analysis, 40, 433–435 (2008).

[31] G. Kresse and J. Furthmüller, Efficient iterative schemes for ab initio total-energy calculations using a plane-wave basis set. Phys. Rev. B, 54, 11169 (1996).

[32] G. Kresse and D. Joubert, From ultrasoft pseudopotentials to the projector augmented-wave method. Phys. Rev. B, 59, 1758 (1999).

[33] J. P. Perdew, K. Burke, and M. Ernzerhof, Generalized gradient approximation made simple. Phys. Rev. Lett., 77, 3865 (1996).

[34] J. Tersoff and D. R. Hamann, Theory of the scanning tunneling microscope. Phys. Rev. B, 31, 805 (1985).

[35] K. Nozawa and Y. Ishii, Electronic structures and stability of Ag-In-Ca surfaces. Journal of Physics: Conference Series, 226, 012030 (2010).

[36] Y. Ishii and T. Fujiwara, Hybridization mechanism for cohesion of Cd-based quasicrystals. Phys. Rev. Lett., 87, 206408 (2001).

[37] H. Euchner, T. Yamada, S. Rols, T. Ishimasa, Y. Kaneko, J. Ollivier, H. Schober, M. Mihalkovic, and M. de Boissieu, Tetrahedron dynamics in the icosahedral quasicrystals i-ZnMgSc and i-ZnAgSc and the cubic 1/1-approximant Zn_6Sc. Journal of Physics: Condensed Matter, 25, 115405 (2013).

[38] C. P. Gómez and S. Lidin, Comparative structural study of the disordered M–Cd_6 quasicrystal approximants. Phys. Rev. B, 68, 024203 (2003).

[39] K. Nishimoto, T. Sato, and R. Tamura, Low-temperature superstructures of a series of Cd_6–M (M= Ca, Y, Sr, Pr, Nd, Sm, Gd, Tb, Dy, Ho, Er, Tm, Yb and Lu) crystalline approximants. Journal of Physics: Condensed Matter, 25, 235403 (2013).

[40] Ph. Ebert, F. Yue, and K. Urban, Surface structures of cleaved icosahedral Al-Pd-Mn single quasicrystals after heat treatment. Phys. Rev. B, 57, 2821 (1998).